ELSEVIER

Cement & Concrete Composites 24 (2002) 477–484

Cement & Concrete Composites

www.elsevier.com/locate/cemconcomp

# Electrical characterisation as a function of frequency: application to aluminous cement during early hydration

Agnès Smith [a,*], Pierre Abélard [b,1], Frédéric Thummen [a], Alexandre Allemand [a]

[a] Groupe d'Etude des Matériaux Hétérogènes (EA 3178), Ecole Nationale Supérieure de Céramique Industrielle, 47 à 73 Avenue Albert Thomas, 87065 Limoges Cedex, France

[b] Laboratoire Science des Procédés Céramiques et Traitements de Surface (UMR 6638), Ecole Nationale Supérieure de Céramique Industrielle, 47 à 73 Avenue Albert Thomas, 87065 Limoges Cedex, France

**Abstract**

Electrical measurement as a function of frequency is a non-destructive technique which has been applied on numerous ceramic based systems such as single crystals, heterogeneous materials or concentrated suspensions of ceramic powders. It is a method for looking at the dynamic response of the system under test. Several approaches have been developed by different authors to give the associated relaxation times based on a single or on a distribution of times. In order to support the interpretation of the dynamic signal, one has to vary the physical or chemical parameters such as temperature, time, concentration and so on. Application of high frequency measurements (1 MHz–1.8 GHz) on aluminous cement pastes (W/C = 0.4) is described. The variations of the capacitance with respect to setting time (from 0 to a few hours after mixing water and cement) and temperature (20 and 30 °C) are related to hydration chronology and to the quantity of formed hydrates. The high frequency response of $C_3AH_6$, which has been prepared by a chemical route, is also discussed.



*Keywords:* Electrical characterisation; High frequency measurements; Calcium aluminate cement

## 1. Introduction

In order to characterise the electrical response of ceramic materials such as capacitors [1], semiconductors [2,3] or cement based systems [4–16], measurements as a function of frequency have been developed. These measurements are based on the study of the dynamic response of the specimen under test. In this paper, we wish to present in the first part some basic principles of frequency measurements and illustrate their application to some materials. The second part of this paper is specifically dedicated to high frequency characterisation (1 MHz–1.8 GHz), as a function of setting time and temperature, of fresh aluminous cement paste. We also present preliminary results on the dielectric behaviour of one hydrate, namely $C_3AH_6$.

## 2. Principle of high frequency measurements

### 2.1. Theory of the linear response

When a step voltage is applied on a component, we usually observe that the current does not take immediately the steady value as predicted by Ohm's law. The current is proportional to the applied voltage, the most general law being an integral relationship:

$$I(t) = \int_{-\infty}^{t} \alpha(t - t')V(t')\,dt', \tag{1}$$

where $\alpha(s)$ is the response function and $t' \leqslant t$, according to the causality principle. If we apply a sine wave voltage of amplitude $V_0$ and pulsation $\omega$, we have $\overline{V} = V_0 \exp(j\omega t)$. [2] Eq. (1) becomes:

* Corresponding author. Tel.: +33-5-5545-2204; fax: +33-5-5579-0998.

*E-mail addresses:* a.smith@ensci.fr (A. Smith), p.abelard@ensci.fr (P. Abélard).

[1] Also Corresponding author.

[2] The applied voltage is indeed real and equal to the real part of $\overline{V}$. The use of complex quantities is assumed to be familiar to the reader.

0958-9465/02/$ - see front matter 
PII: S0958-9465(01)00079-8

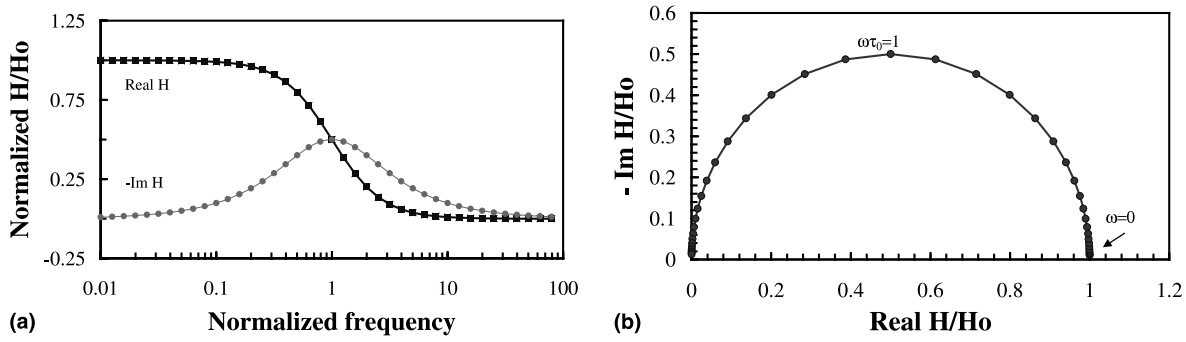


Fig. 1. (a) Variations of the real and imaginary parts of $H/H_0$ as a function of frequency according to Eq. (4). (b) Variations of the imaginary part of $H/H_0$ as a function of the real part: representation in Bode's plane.

$$\bar{I}(t) = V_0 \int_{-\infty}^{t} \alpha(t-t') \exp(j\omega t')\,\mathrm{d}t' = V_0 \exp(j\omega t) \int_0^{+\infty} \alpha(s) \exp(-j\omega s)\,\mathrm{d}s. \quad (2)$$

Due to the linearity property, the response is also a sine wave with the same pulsation but the ratio of current to voltage, called the admittance $Y(\omega)$, is a complex quantity:

$$Y(\omega) = \frac{\bar{I}}{\bar{V}} = \int_0^{+\infty} \alpha(s) \exp(-j\omega s)\,\mathrm{d}s \quad (3)$$

which becomes real in the limit of zero frequency: $Y(0) = 1/R$.

One possible response function is a Debye's one, noted $\alpha_h(s)$. [3] In that case, the response function is a first-order differential equation, i.e. an exponentially decreasing function of time:

$$\alpha_h(s) = \tau_0 H_0 \exp\left(-\frac{s}{\tau_0}\right) \Longleftrightarrow H(\omega) = \frac{H_0}{(1+j\omega\tau_0)}. \quad (4)$$

The variations of the real and imaginary parts of $H$ are depicted in Fig. 1(a) in a semi-logarithmic system of coordinates. The imaginary part, $-\mathrm{Im}\,H$ indeed, is a Lorentzian, centred on $\omega\tau_0 = 1$. Most of the variations occur in a frequency range of approximately three decades around $\tau_0^{-1}$. The electrical properties are dispersive in that range. For higher frequencies, the response is very small while at lower frequencies, $H$ is constant and equal to $H_0$ (during one period $T = 2\pi/\omega$, there is sufficient time to establish a steady regime). It is also customary to plot the data in Bode's plane, i.e. ($-\mathrm{Im}\,H$, $\mathrm{Re}\,H$). The corresponding figure is a semicircle centred on the real axis (Fig. 1(b)). Very often, one has to consider a distribution of relaxation times:

$$H(\omega) = H_0 \int \frac{G(Ln\tau)}{1+j\omega\tau}\,\mathrm{d}Ln\tau. \quad (5)$$

[3] In this paragraph, $H(\omega)$ can be the admittance, the impedance or any appropriate response.

The effect is to widen and deform the Lorentzian shape of ($-\mathrm{Im}\,H$). Inverting Eq. (5) in order to get the distribution $G(Ln\tau)$ from the experimental data is difficult. Some specific cases can be solved analytically, for instance:

$$H(\omega) = \frac{H_0}{1+(j\omega\tau)^n} \Longleftrightarrow G(Ln\tau) = \frac{1}{2\pi} \frac{\sin[\pi(1-n)]}{\cosh\{n\log(\tau_0/\tau)\} - \cos[\pi(1-n)]}. \quad (6)$$

A representation is given in Fig. 2(a). In Bode's plane, the diagram is a semicircle depressed below the real axis by an angle $\theta = (1-n)(\pi/2)$, as shown in Fig. 2(b). Computer software can also be used to extract $G(Ln\tau)$ from the experimental data. It should be noted that the theory of the linear response is a mathematical description of the dynamic response of the system under test. Without a physical model, the response function gives no information other than the dynamic. Even the modelisation with a distribution of time constants is part of the interpretation; in that case, we assume that an elementary mechanism exists which can be described by a first-order differential equation and that the deviation from a Debye type behaviour must be correlated to some disorder in the system. An interpretation which could be equally true consists of describing the dynamic by a more complex differential equation without any disorder present. The only way to ascertain an interpretation is to vary parameters such as temperature, water content, concentration, and so on, and analyse their effects on the dynamic parameters.

### 2.2. Examples of applications

For single crystals [17,18], the admittance of a pure homogeneous material is given by the following relation:

$$Y(\omega) = \frac{A}{t}\{\sigma_0 + j\varepsilon\omega\}, \quad (7)$$

where $\sigma_0$ is the electrical conductivity, $\varepsilon$ the dielectric permittivity of the material, and $A/t$ (= area/thickness)

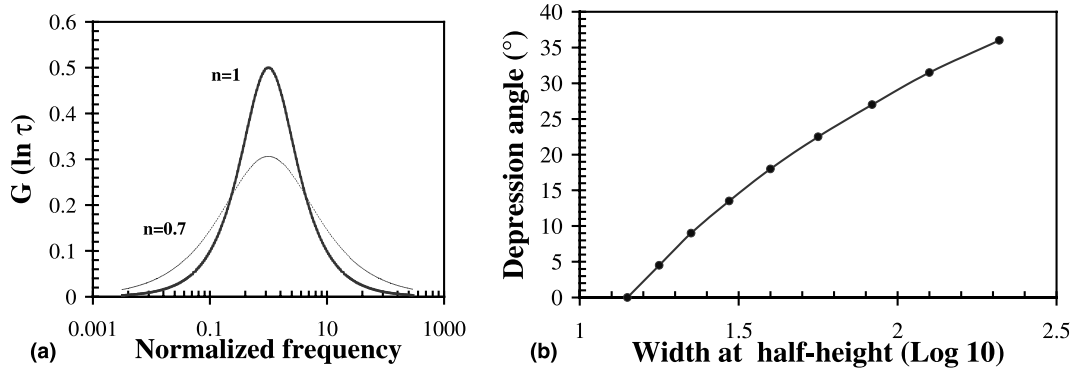


Fig. 2. (a) Representation of the distribution function, described by Eq. (6), for two values of the $n$ coefficient; it can be noted that for $n = 1$, the distribution corresponds to the distribution function for Debye' model. (b) Depression angle as a function of $n$ for the representation of the semi-circle in Bode's plane.

the geometrical factor of the sample in the case of a disc shape. The material can be represented by a resistor and a capacitor in parallel. The first term arises from the long-range motions of charge carriers, while the second term describes the polarisation of matter. The case of single crystals is probably the easiest situation to deal with.

In the case of heterogeneous materials, different models have been developed to calculate the admittance. One approach is Maxwell–Wagner's model where spherical inclusions are dispersed in a matrix. It is relevant for describing the electrical response of ceramics which have been sintered at high temperatures in the presence of a liquid phase.

Another approach is the effective medium theory; the material is supposed to be a mix of two types of grains. The admittance is the solution of the following equation:

$$\sum_i p_i \cdot \frac{Y - (t/A)\sigma_i}{2Y + (t/A)\sigma_i} = 0, \tag{8}$$

where the symmetry with respect to $\sigma_1$ and $\sigma_2$ is apparent. This equation predicts quite well the percolation effect.

Another interesting system to characterise electrically is a concentrated suspension of powder. This has been done in the case of oxides in water [19] where the surface of the particles is charged or neutral depending on the pH. Let us assume for convenience that, altogether, the surface is negatively charged. Positive ions in the solution, called counterions, are attracted and form a diffuse layer of thickness $1/\kappa$, typically of a few nanometers. The thickness is related to other parameters through the following equation:

$$\kappa^2 = \frac{q^2 C_0}{\varepsilon k_B T}, \tag{9}$$

where $q$ is the charge, $C_0$ the concentration of counterions in the electrolyte (i.e. outside the diffuse layer), and $\varepsilon$ is the permittivity of the solvent, which screens the electric field created by the negative charge.

If we apply a step voltage, the following sequence of events occurs ([20] and Fig. 3): almost instantaneously ($\tau \cong 10^{-13}$–$10^{-14}$ s), the grains, assumed to be insulators, polarise, followed by the water molecules ($\tau \cong 10^{-11}$ s). At this time, each grain is like a microscopic dipole and contributes a dipolar electric field. Its component tangent to the surface drives the counterions into

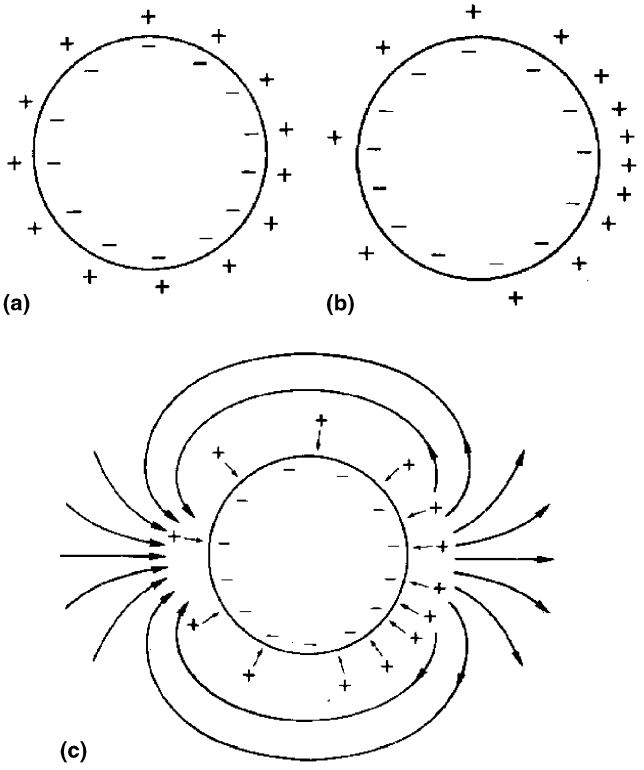


Fig. 3. Schematic representation of the electrical environment around a grain of powder when (a) $t \approx 0$ s, (b) $t \approx \tau_1$ (associated to the formation of dipoles) and (c) $t \approx \tau_2$ (corresponding to diffusion flow in the electrolyte).

the diffuse layer, which accumulate at the pole of the spherical grain, defined by the direction of the applied electric field. On the opposite pole, the diffuse layer is depleted of counterions: a macroscopic dipole has formed. According to O'Brien's analysis [20,21], this process is a Debye one and the characteristic time, $\tau_1$, is of the order of $1/(D\kappa^2)$ where $D$ is the diffusivity of the counterions. The difference in concentrations at the two poles initiates a diffusion flow in the electrolyte in order to suppress it. [4] The characteristic time, $\tau_2$, is of the order of $a^2/D$ if $a$ is the radius of the grains. When $\tau_1/\tau_2 = (\kappa a)^2$ is large, the two processes occur in quite different time intervals. A schematic representation of the different processes is given in Fig. 3. Several attempts have been done to measure the admittance of the suspension in the low frequency range, but they have encountered numerous difficulties: electrode effects give an important contribution. If the volume fraction of powder is low, the contribution of the surface conductivity is small and if this fraction is high, then interferences between grains occur. Measurements at high frequencies, in the microwave range, are rare because of the technique involved. However, they are attractive because electrode effects are negligible and the motion of the ions is restricted to the diffuse layers. This permits the study of concentrated suspensions and we can get information specifically about the solid–liquid interface.

As a concluding remark, high frequency measurements carried out on concentrated ceramic suspensions have shown that it is possible to get information concerning solid–liquid interfaces. We have applied this technique to aluminous cement pastes during hydration. In that case, the parameter which varies is the setting time. The second part of this paper is devoted to the description of the evolution of the dielectric response as hydration proceeds in an aluminous cement. Preliminary results on one pure hydrate, namely $C_3AH_6$, are also presented.

## 3. High frequency characterisation (1 MHz–1.8 GHz) on cement based compositions

### 3.1. Case of an aluminous cement at the early age: effect of setting time

#### 3.1.1. Preparation procedure

The tested material is an aluminous cement (average particle size: 50 μm; density : 2.90–3.05 g cm$^{-3}$; $Al_2O_3$: 69.8–72.2 wt%; CaO: 26.8–29.2 wt%). It is mixed with distilled water in a Perrier blender for 6 min with a water to cement weight ratio, W/C, equal to 0.4. After this step, the paste is cast in a cell which has been specifically designed for high frequency measurements. A K-thermocouple is immersed in the paste. The electrical response is followed just after mixing and for two temperatures (20 and 30 °C).

#### 3.1.2. Principle of electrical characterisation at high frequency

The measurements were carried out between 1 MHz and 1.8 GHz with the 4291A Hewlett-Packard apparatus using a coaxial line. Instead of the usual vector-voltage–current-ratio measurement method (usable at low frequencies), the principle is to measure the reflection coefficient of an electromagnetic wave sent on the tested sample. The HP 4291A applies a measurement frequency test signal to the sample which is terminated at the test port and detects the vector-voltage-ratio of the reflected wave, $V_{\text{ref}}$, to the incident wave, $V_{\text{inc}}$, to measure the reflection coefficient. The complex reflection coefficient, $\Gamma^*$, is defined as:

$$\Gamma^* = \frac{V_{\text{ref}}}{V_{\text{inc}}} = \Gamma_X + \mathrm{i}\Gamma_Y. \tag{10}$$

The complex reflection coefficient value and the normalised complex impedance value of the sample, $Z_{\text{R}}^*$, are related by the following formula:

$$Z_{\text{R}}^* = \frac{1+\Gamma^*}{1-\Gamma^*}, \tag{11}$$

where $Z_{\text{R}}^*$ is defined as:

$$Z_{\text{R}}^* = \frac{Z^*}{Z_0}, \tag{12}$$

where $Z^*$ is the complex impedance of the tested material and $Z_0$ is the characteristic impedance of the coaxial line (50 Ω).

The next stage is to relate the complex dielectric permittivity, $\varepsilon^*$, of the cement with its complex impedance. For an alternating field, the complex permittivity is given by:

$$\varepsilon^* = \varepsilon' - \mathrm{i}\varepsilon'' = \varepsilon_0\left(\varepsilon'_{\text{R}} - \mathrm{i}\varepsilon''_{\text{R}}\right), \tag{13}$$

where $\varepsilon_0$ is the permittivity of vacuum and $\varepsilon'$ (resp. $\varepsilon'_{\text{R}}$) and $\varepsilon''$ (resp. $\varepsilon''_{\text{R}}$) are the real and imaginary parts of the permittivity (resp. relative permittivity). $\varepsilon^*$ is related to the complex admittance, $Y^*$ (where $Y^* = 1/Z^*$), as follows:

$$\frac{Y^*}{\mathrm{i}\omega} = \varepsilon^* L(\omega) = \varepsilon_{\text{R}}^* \varepsilon_0 L(\omega), \tag{14}$$

where $L(\omega)$ is a geometrical factor which takes into consideration the edge effects as specified by Hewlett-Packard.

The experimental cell is presented in Fig. 4. It consists of a coaxial line at the end of which there is a cylindrical

[4] A diffusion type cannot be described by a first-order differential equation and the admittance is a complicated function of $\sqrt{\omega}$.

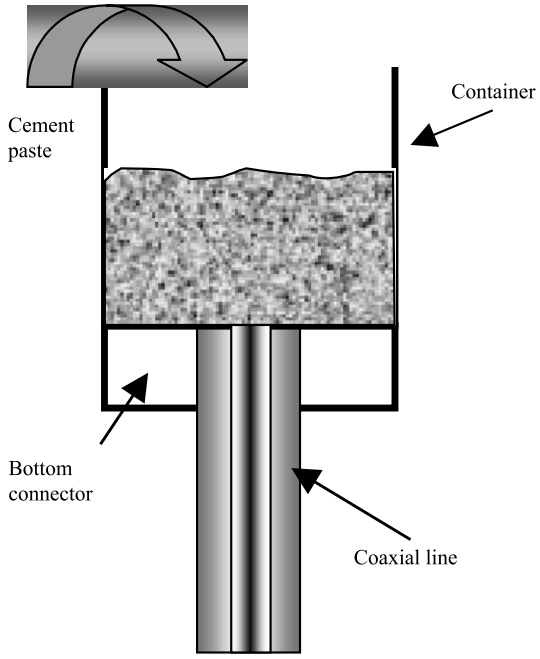


Fig. 4. Schematic representation of the measurement cell.

container filled with cement paste. This cell is enclosed in a chamber where the temperature is controlled.

### 3.1.3. Results and discussion

In Fig. 5 are represented the capacity variations at 20 and 30 °C as a function of setting time for different frequencies. Similar measurements but at lower frequencies (20 Hz–300 kHz) have been carried out by McCarter et al. [4,5]. In that case, the material was a Portland cement prepared with a W/C ratio equal to 0.25–0.35. The characterisation was done at 25 °C and 75% relative humidity for 24 h. In the present case, three zones can be distinguished in Fig. 5: in zone I, the capacitance increases slightly at the lowest frequencies as a function of setting time for measurements at 20 °C, and remains fairly constant for measurements at 30 °C. For the highest frequencies, the capacitance stays constant whatever the temperature of measurement is. Zone II corresponds to the duration where the capacity goes through a maximum at low frequency and decreases progressively at high frequency. Lastly, in zone III and at 20 °C, the capacitance decreases slightly at the lowest frequency end and remains constant at the highest frequencies. In the case of measurements at 30 °C, there is little variation of the capacity in zone III as a function of setting time whatever the frequency is.

In the same figure are reported the temperature variations. At the beginning and for characterisations done at 20 °C, there is a slight endothermal phenomenon which can be associated to the formation of primary hydrates [22]. At 30 °C, the nucleation of hydrates does not seem to induce an endothermal phenomenon. The massive precipitation of hydrates is characterised by an exothermal peak [23] whose amplitude depends on the volume and environment of the material. Depending on the temperature at which the experiment has been carried out (20 or 30 °C), there is not necessarily a coincidence between the temperature and capacitance variations, especially in zone II. A simple explanation can be proposed: temperature is a macroscopic information which depends on the volume of material and also on the environment. Electrical characterisation gives a response at a microscopic scale since it is associated to electrical phenomenon occurring at solid–liquid interfaces.

Concerning the general shape of the curves, a possible interpretation of the three zones is the following:

- In zone I, there is a dissolution of calcium ions in the form of $Ca^{2+}$ and aluminium ions in the form of aluminate ions $AlO_2^-$. The difference in capacitance variations at the lowest frequencies between measurements at 20 and 30 °C could be due to differences in dissolution kinetics of these two ions as a function of temperature and also in the nucleation mechanism of primary hydrates with respect to temperature.

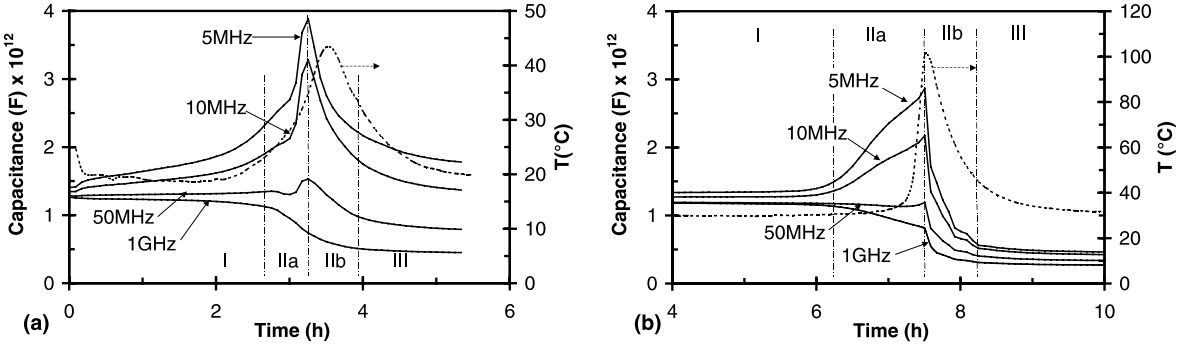


Fig. 5. Capacitance and temperature variations as a function of time for different frequencies. Temperature of the environment: 20 °C (a), and 30 °C (b).

- Zone II can be separated into two regions (IIa and IIb) based on the variations at the lowest frequencies. In zone IIa, the capacity increases drastically. It could be related to a massive precipitation of hydrates. If this precipitation is homogeneous (i.e. starts from nuclei contained in the water), it means that new surfaces are created, which implies a greater and greater electrical capacitance. When hydrates start coalescing, surfaces meet each other and the net result is a decrease in the number of free surfaces, which corresponds to a decrease in capacitance (zone IIb). The difference between measurements at 20 and 30 °C concerns the shape of the curves which could be explained by the fact that hydrates grow with different morphologies and develop different chemical formulas [24]. Moreover, zone II is delayed by about 3 h in the case of measurements done at 30 °C compared to those at 20 °C. This could be explained by a lengthening of setting time which is supposed to occur around 30 °C [22].
- In zone III, the capacity varies less as a function of setting time. Since the cement is set, it is less likely that the electrical environment at the interfaces around the hydrates or the cement particles evolves very rapidly with time.

In the following, we wish to discuss how it is possible to correlate the variations of the volumic percentage of each phase, namely water, cement and hydrates, with respect to capacity variations at high frequency. For this analysis, we need to know $\varepsilon_\infty$. Using Provencher's approach [25,26], we can calculate $\varepsilon_\infty$ for the paste at different setting times and we notice that $\varepsilon_\infty$ is very close to the value measured at 1 GHz.

At 20 °C, during the first 24 h, hydration can be simply described by the following reaction:

$$CA + 10H \rightarrow CAH_{10}. \tag{15}$$

From thermogravimetric measurements carried out on specimens at increasing times, we can calculate the volumic percentages of water, $p_{H_2O}$, cement, $p_{CA}$, and hydrate, $p_{CAH_{10}}$ [27]. The results are presented in Fig. 6(a). We can notice in this figure that, between 2 and 4 h, $CAH_{10}$ progressively becomes the major phase. These variations have to be compared with capacitance variations at high frequency which are reported in Fig. 5(a). The next step is to know $\varepsilon_\infty$ for each phase. At 20 °C, for water, we have: $\varepsilon_{H_2O} = 80$. Just after mixing, we assume that $p_{CAH_{10}} = 0$vol%. $\varepsilon$ measured at 1 GHz on the paste and at that stage corresponds to a mixture of water and CA. Since $\varepsilon_{H_2O}$ is known, we can deduce $\varepsilon_{CA} = 16.7$. In order to estimate $\varepsilon_{CAH_{10}}$, we have taken the experimental values of $\varepsilon$ at 21 h. Knowing the proportion of each phase at 21 h, we can estimate $\varepsilon_{CAH_{10}} = 8.8$. Using a percolation model, $\varepsilon$ at high frequency can be calculated from Eq. (8):

$$p_{H_2O}\frac{\varepsilon - \varepsilon_{H_2O}}{2\varepsilon + \varepsilon_{H_2O}} + p_{CA}\frac{\varepsilon - \varepsilon_{CA}}{2\varepsilon + \varepsilon_{CA}} + p_{CAH_{10}}\frac{\varepsilon - \varepsilon_{CAH_{10}}}{2\varepsilon + \varepsilon_{CAH_{10}}} = 0 \tag{16}$$

with

$$p_{H_20} + p_{CA} + p_{CAH_{10}} = 100\text{vol}\%. \tag{17}$$

The variations of the calculated values are plotted in Fig. 6(b) together with the variations of the value deduced from capacitance measurements at 1 GHz (Fig. 5(a)). We notice a good correlation between the two sets of points. It means that the experimental determination of the permittivity could enable to have an in situ signature of the chemical composition of the paste. In order to go further in this approach, we need to have a good knowledge of particle morphology since the high frequency response is directly linked to surface phenomena.

### 3.2. Preliminary results on the high frequency response of chemically synthesised $C_3AH_6$

In this last section, we wish to present the dielectric response of a pure hydrate. Indeed, since an aluminous cement is a composite material of anhydrous and hydrated phases, it is useful to know the frequency response of each constituent. Our first effort has been focussed on $C_3AH_6$ which is the thermodynamically stable hydrate [24,28].

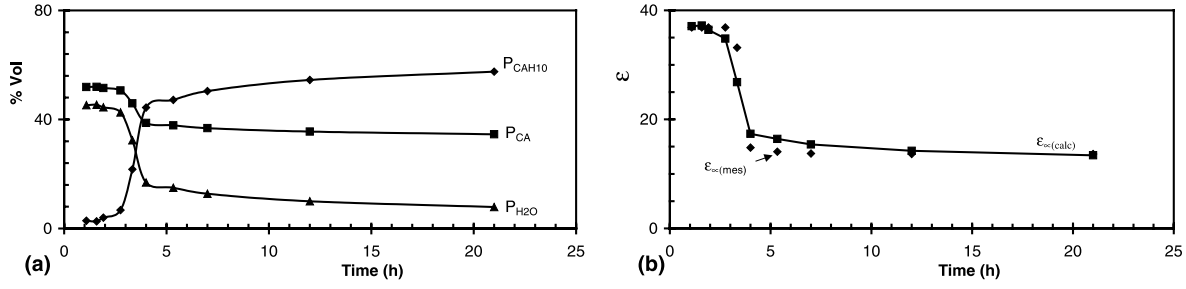


Fig. 6. (a) Volumic percentage of water, CA and $CAH_{10}$, estimated from thermogravimetric measurements [27]. (b) Comparison between the calculated and the experimental values of $\varepsilon$ as a function of time for the hydration reaction described by (15).

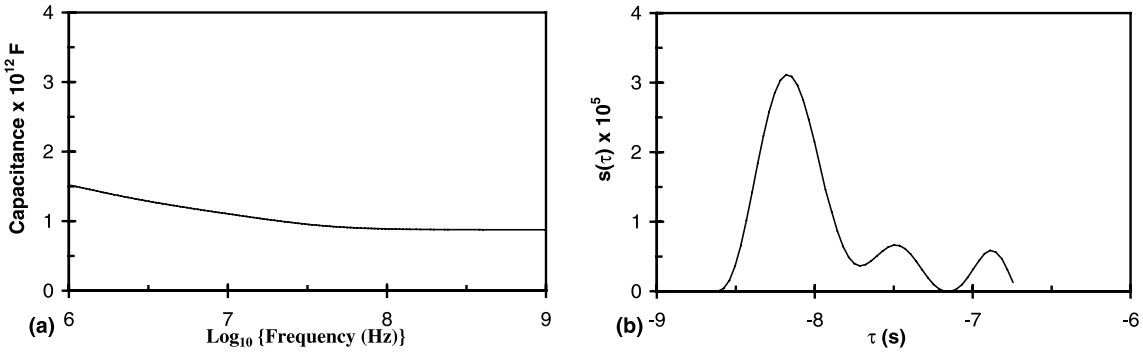


Fig. 7. (a) Capacitance variations as a function of frequency for $C_3AH_6$. (b) Analysis of the corresponding relaxation times [25,26].

$C_3AH_6$ can be prepared by hydration of CA or $C_3A$ at $T > 50$ °C or by conversion of $CAH_{10}$ and $C_2AH_8$. In order to synthesise $C_3AH_6$ we have used a chemical method derived from a self-propagation combustion method [29]. It is based on the combustion of calcium nitrate and aluminium nitrate in the presence of citric acid according to the following reaction:

$$3Ca(NO_3)_2 + 2Al(NO_3)_3 + 10/3C_6H_8O_7 \rightarrow 20CO_2 + 6N_2 + (CaO)_3Al_2O_3 + 40/3H_2O. \quad (18)$$

Stoichiometric quantities of each starting material are mixed in water, heated at 80 °C until a gel is obtained. This gel is then calcined under an air flow at 450 °C for 15 min. The resulting product is heated at 1050 °C. The final powder consists only of crystallised $C_3A$. In order to hydrate $C_3A$, it is mixed with water and heated at 120 °C under 3 bars. This method enables to obtain a powder which is crystallised $C_3AH_6$. At this stage, it is useful to note that this molecule is in fact a hydroxide whose chemical formula can be re-written as $[Ca(OH)_2]_3[Al(OH)_3]_2$.

Prior to electrical measurements, this hydrate powder has been mixed with water for wetting the grains. Electrical characterisations of this hydrate have been carried out as a function of frequency. The capacitance variations show a typical behaviour of a dielectric material where the capacitance decreases from high to low values when the frequency increases [30] (Fig. 7(a)). A numerical analysis has been carried out using Provencher's software and the results are presented in Fig. 7(b). The interest of such an approach is to be able to know the corresponding spectrum of relaxation times associated with the capacitance variations. In the domain of interest, three peaks can be distinguished: the one at the shortest time could be attributed to the relaxation of water molecules. The two other peaks could correspond to the relaxation of hydroxyl groups which are part of $C_3AH_6$ and which are located on the surface of the particles. By analogy to the work which has been done on concentrated ceramic powder suspensions [19], a possible interpretation of these two peaks is the following: the one at the longest time is linked to electrical phenomenon in Stern's layer and in particular to the capacitance of the grain surface which is composed of hydroxyl groups. The peak at the intermediate time corresponds to electrical phenomenon occurring in the diffuse layer. Further work is still needed in this direction (i.e. electrical response of pure systems).

## 4. Conclusion

In the first part of this paper, we have presented the principle of electrical measurements as a function of frequency. We have specifically focussed on the fact that these measurements correspond to a dynamic response of the system under test and that mathematical models have been developed to describe this dynamic response. Nevertheless, a complete interpretation of these signals implies to vary physical or chemical parameters such as time, temperature, pH, concentration and so on. In the second part, we discuss the results concerning the high frequency characterisation of a fresh aluminous cement paste for increasing setting times. The dielectric response enables to propose the following chronology for hydrate formation: after the first stage of dissolution and nucleation, hydrates grow from the solution, which corresponds to an increase of the capacitance at low frequency. As hydration advances, these hydrates start either coalescing between themselves or meet anhydrous grains, which could explain the decrease in capacitance. Lastly, results on one pure hydrate, i.e. $C_3AH_6$, is an interesting opening to go further into the chemical interpretation of our signals.

## References

[1] Ravez J, Bonnet JP, Simon A, Denage C, Miane JL. Correlations between processing parameters and relaxation frequencies in

$SrTiO_3$-type grain boundary layer ceramics. J Phys Chem Solids 1990;51(8):957–60.
[2] Smith A, Baumard JF, Abélard P. Ac impedance measurements and *V–I* characteristics for Co-, Mn-, or Bi-doped ZnO. J Appl Phys 1989;65(12):5119–25.
[3] Tanaka J, Baumard JF, Abélard P. Non-linear electrical properties of grain boundaries in an oxygen-ion conductor $(CeO_2 \cdot Y_2O_3)$. J Am Ceram Soc 1987;70(9):637–43.
[4] McCarter WJ, Afshar AB. Monitoring the early hydration mechanisms of hydraulic cement. J Mater Sci 1988;23:488–96.
[5] McCarter WJ, Ezirim HC. Monitoring the early hydration of pozzolan-$Ca(OH)_2$ mixtures using electrical methods. Adv Cem Res 1998;10(4):161–8.
[6] McCarter WJ, Garvin S, Bouzid N. Impedance measurements on cement paste. J Mater Sci Lett 1988;7:1056–7.
[7] Gu P, Xie P, Fu Y, Beaudoin JJ. AC impedance phenomena in hydrating cement systems: the drying–rewetting process. Cem Concr Res 1994;24:89–91.
[8] Gu P, Beaudoin JJ. Dielectric behaviour of hardened cementitious materials. Adv Cem Res 1997;9(33):1–8.
[9] Yoon SS, Kim SY, Kim HC. Dielectric spectra of fresh cement paste below freezing point using an insulated electrode. J Mater Sci Lett 1994;29:1910–4.
[10] Zhang X, Ding XZ, Ong CK, Tan BTG, Yang J. Dielectric and electrical properties of ordinary portland cement and slag cement in the early hydration period. J Mater Sci 1996;31:1345–52.
[11] El Hafiane Y, Smith A, Abélard P, Bonnet JP, Abélard P, Blanchart P. Electrical characterisation at aluminous cement at the early age in the 10 Hz–1 GHz frequency range. Cem Concr Res 2000;30:1057–62.
[12] El Hafiane Y, Smith A, Abélard P, Bonnet JP, Blanchart P. Dielectric characterization at high frequency of a portland cement at the early stages of hydration. Ceramics–Silikaty 1999;43(2): 48–51.
[13] Christensen BJ, Tate Coverdale R, Olson RA, Ford SJ, Garboczi EJ, Jennings HJ, et al. Impedance spectroscopy of hydrating cement-based materials: measurements, interpretation, and application. J Am Ceram Soc 1994;77(11):2789–804.
[14] Miura N, Shinyashiki N, Yagihara S, Shiotsubo M. Microwave dielectric study of water structure in the hydration process of cement paste. J Am Ceram Soc 1998;81(1):213–6.
[15] MacPhee DE, Sinclair DC, Stubbs SL. Electrical characterization of pore reduced cement by impedance spectroscopy. J Mater Sci Lett 1996;15:1566–8.
[16] Keddam M, Takenouti H, Novos XR, Andrade C, Alonso C. Impedance measurements on cement paste. Cem Concr Res 1997; 27(8):1191–201.
[17] Scher H, Lax M. Stochastic transport in a disordered solid. I Theory. Phys Rev B 1973;7(10):4491–501.
[18] Fontanella J, Jones DL, Andeen C. Dipolar complexes in rare-earth-doped strontium fluoride. Phys Rev B 1978;18(8):4454–61.
[19] Bach G. Etude de la dispersion en fréquence de la conductivité électrique de suspensions céramiques concentrées. Thèse de Doctorat, Université de Limoges, Limoges, France, 1998.
[20] Lyklema J. In: Fundamentals of interface and colloid science: solid–liquid interfaces, vol. II. New York: Academic Press; 1995.
[21] O'Brien RW. The high frequency dielectric dispersion of a colloid. J Colloid Interface Sci 1986;113(1):81–93.
[22] Mangabhai RJ. In: Calcium aluminate cements. London: E&FN Spon, Chapman & Hall; 1990. p. 39–96.
[23] Neville AM. Properties of concrete. New York: Wiley; 1973.
[24] Scrivener KL, Cabiron JL, Letourneux R. High-performance concretes from calcium aluminate cements. Cem Concr Res 1999; 29:1215–23.
[25] Provencher SW. A constrained regularisation method for investing data represented by linear algebraic or integral equations. Comput Phys Commun 1982;27:213–27.
[26] Provencher SW. A general purpose constrained regularisation program for investing noisy linear algebraic or integral equations. Comput Phys Commun 1982;27:229–42.
[27] Chotard T, Gimet-Bréart N, Smith A, Fargeot D, Bonnet JP, Gault C. Application of ultrasonic testing to describe the hydration of calcium aluminate cement at the early age. Cem Concr Res 2001;31:405–12.
[28] Richard N. Structure et propriétés élastiques des phases cimentières à base de mono-aluminate de calcium. Thèse de Doctorat, Université de Paris VI, Paris, France, 1996.
[29] Cüneyt A. Chemical preparation of the binary compounds in the calcia–alumina system by self-propagation combustion synthesis. J Am Ceram Soc 1998;81(11):2853–63.
[30] Kingery WD. In: Introduction to ceramics. New York: Wiley; 1975. p. 927.